General Disclaimer

One or more of the Following Statements may affect this Document

- This document has been reproduced from the best copy furnished by the organizational source. It is being released in the interest of making available as much information as possible.

- This document may contain data, which exceeds the sheet parameters. It was furnished in this condition by the organizational source and is the best copy available.

- This document may contain tone-on-tone or color graphs, charts and/or pictures, which have been reproduced in black and white.

- This document is paginated as submitted by the original source.

- Portions of this document are not fully legible due to the historical nature of some of the material. However, it is the best reproduction available from the original submission.

NASA

Technical Memorandum 79537

A Beaming Model of the Io-Independent Jovian Decameter Radiation Based on Multipole Models of the Jovian Magnetic Field

Melvyn L. Goldstein, Aharon Eviatar and James R. Thieman

APRIL 1978

National Aeronautics and Space Administration

Goddard Space Flight Center
Greenbelt, Maryland 20771

TM 79537

A BEAMING MODEL OF THE IO-INDEPENDENT JOVIAN DECAMETER RADIATION BASED ON MULTIPOLE MODELS OF THE JOVIAN MAGNETIC FIELD

Melvyn L. Goldstein
Laboratory for Extraterrestrial Physics
NASA/Goddard Space Flight Center

Aharon Eviatar
Department of Geophysics and Planetary Sciences
Tel-Aviv University

and

James R. Thieman*
Laboratory for Extraterrestrial Physics
NASA/Goddard Space Flight Center

Submitted to *The Astrophysical Journal*

NASA/GODDARD SPACE FLIGHT CENTER
Greenbelt, Maryland

*NRC/NAS Resident Postdoctoral Research Associate

CONTENTS

ILLUSTRATIONS

ILLUSTRATIONS

A BEAMING MODEL OF THE IO-INDEPENDENT JOVIAN DECAMETER RADIATION BASED ON MULTIPOLE MODELS OF THE JOVIAN MAGNETIC FIELD

Melvyn L. Goldstein
Aharon Eviatar
and
James R. Thieman

ABSTRACT

A geometrical model is presented in which the apparent source locations of the Io-independent decameter radiation are computed. The calculations assume that the radiation is produced by stably trapped electrons radiating near the local electron gyrofrequency and that the emission is then beamed onto a conical surface. The maximum occurrence probability of noise storms is associated with regions in the Jovian magnetosphere where the axis of the emission cone is most inclined toward the Jovian equatorial plane. The calculations utilize and compare two of the octupole spherical harmonic expansions of the Jovian magnetic field constructed from data accumulated by the fluxgate and vector helium magnetometers on board Pioneer 11.

A BEAMING MODEL OF THE IO-INDEPENDENT JOVIAN DECAMETER RADIATION BASED ON MULTIPOLE MODELS OF THE JOVIAN MAGNETIC FIELD

I. INTRODUCTION

Jupiter's low frequency radio emission at decameter (DAM) wavelengths has two components. In the first, the occurrence probability of a noise storm depends on both the Jovian central meridian longitude (CML) that faces Earth and the orbital phase of the innermost Galilean satellite, Io. Secondly there is a significant probability of observing DAM radiation at particular central meridian longitudes, independent of Io control. [For a recent detailed review of the observations the reader is referred to Carr and Desch (1976).] In this paper, we concentrate on this Io-independent component of the decameter radiation, adopting the viewpoint that although the origins of the Io-controlled and Io-independent radiation are both profoundly influenced by the local properties of the Jovian magnetic field, the physical emission mechanisms and source locations of the two components can be distinct.

The Jovian magnetic field determines the source locations of the radiation, and the magnetic field measurements made in the inner magnetosphere on Pioneer 11 have greatly increased our knowledge of the detailed structure of that field. Models have been constructed which permit extrapolations of the field down to the Jovian cloud tops. The measurements indicate that within six Jovian radii (R_J), models of the Jovian magnetic field will reasonably fit the data if they include internal source terms up to the octupole. The surface fields that one infers in the northern hemisphere reach 14G, while in the south the maximum is approximately 10G. In a 14G field, the local electron gyrofrequency is 39 MHz – very close to the maximum observed frequency of the Io-controlled

DAM component (Warwick 1964). The highest electron gyrofrequency in the southern hemisphere is 29 MHz -- close to the maximum of the Io-independent component (Wilson, Warwick, and Libby 1968; Thieman and Smith 1978). We shall assume that this 29 MHz cutoff in the Io-independent component is a physical effect not an observational limitation created by the combined effects of limited antenna system sensitivity and the greater intensity of the Io-controlled component, as was suggested recently by Desch (1976).

Based on this evidence, we conclude that the decameter radiation is produced near the local electron gyrofrequency and, furthermore, that emission associated with the Io-independent component originates from electrons stably trapped in the Jovian magnetosphere, for trapped particles cannot reach fields higher than the maximum in the south. Goldstein and Eviatar (1972) proposed that trapped electrons could produce the Io-independent DAM via a cyclotron instability driven by a loss-cone distribution. However in that paper, a centered dipole field was assumed with a field strength far in excess of what we now know to exist. Thus, clearly our increased knowledge demands some modification of those ideas. Using the high-order multipole models of the magnetic field to construct the beaming model developed below, we can now estimate the longitudinal locations of the radiation sources in the Jovian magnetosphere. From these source positions, the longitudes from which radiation is beamed toward Earth can be found, and one can proceed to develop more complete theories of the emission mechanism. Such a theory is proposed in the accompanying paper (Goldstein and Eviatar 1978).

Implicit in our analysis is the assumption that the DAM escapes in the R-X mode, near the local electron cyclotron frequency. In fact, we will be most interested in the free escape propagation band (Band III) for which the angular frequency ω exceeds ω_R,

where (Stix 1962)

$$\omega_R = \tfrac{1}{2}|\Omega_e|[1 + (1 + 4\omega_{pe}^2/\Omega_e^2)^{1/2}] \qquad (1)$$

in which ω_{pe} is the local electron plasma frequency, and $\Omega_e \equiv -|e|B/Mc$ is the electron Larmor frequency. The emission frequency will then be close to the gyrofrequency as long as $\omega_{pe} \ll |\Omega_e|$. This implies a local electron density, N_e, less than 10^6 cm^{-3}, which seems likely everywhere in and above the Jovian ionosphere (Fjeldbo, et al. 1976; and Atreya and Donahue 1976).

In the development presented below we examine the implications of the assumption that stably trapped electrons are the exciters of the Io-independent DAM. This can be done regardless of the particular instability mechanism.

II. TRAPPED ELECTRONS IN A MULTIPOLE FIELD

a) Source Locations

In our analysis we have utilized several models of the Jovian magnetic field to examine the sensitivity of our conclusions to the different extrapolations of Pioneer 11 data to the very low altitudes where 10-30 MHz gyrofrequencies are encountered. The models we have used include the O_4 model of Acuña and Ness (1976), containing three internal (I) and no external (E) sources, and the P11(I3-E0) and P11(I3-E1) models proposed by Smith, Davis, and Jones (1976). In the last, because we wished to utilize a time-independent model in a frame rotating with the interior sources, we discarded the $\overline{g}_1^{\,1}$ and $\overline{h}_1^{\,1}$ exterior source coefficients as recommended by Smith et al., leaving only the $\overline{g}_1^{\,0}$ exterior coefficients. Surface maps of the magnetic field computed from all the models are very similar, especially in the northern hemisphere. The most significant difference is the strong tendency of the Smith et al. models to place the highest southern hemisphere fields at higher System III (1965) longitude, λ_{III}, than does the O_4 model (330° compared to 255° in the O_4 model). As we shall see, the accessibility of trapped electrons to regions of high gyrofrequency is quite sensitive to the relative locations of the high field regions in the two hemispheres. Consequently, we have found it necessary to present some of our conclusions in terms of both the O_4 and P11(I3-E1) models. (In general, the P11(I3-E0) model is very similar in most respects to P11(I3-E1)). To simplify further reference to the various Smith et al. models, we will denote the P11(I3-E1) model as the "JPL" model, and continue to use "O_4" to designate the Acuña and Ness model.

The locations in the Jovian magnetosphere that give rise to a particular gyrofrequency are found by integrating the equations describing the trace of a magnetic field

line in spherical coordinates. The integration begins at some point (r,ϕ) in the zenographic equatorial plane and proceeds to calculate $B(r,\theta,\phi)$ down to the cloud tops in the northern and southern hemispheres. The maximum mirror field, B_M, associated with a particular field line is then the lower of the magnetic field values at one of the two ends of the field line. [In locating the foot of a field line, one must include the planetary oblateness. For the radial distance of the cloud tops, we have used (Kahle, Kern, and Vestine 1964)

$$R/R_{\mathcal{U}} = (1 + \epsilon \cos^2 \theta)^{-1/2} \qquad (2)$$

with $\epsilon = 0.14371$ (Anderson, Null and Wong 1974), where θ is colatitude and $R_{\mathcal{U}} = 71{,}372$ km.] The gyrofrequency, f_M, corresponding to B_M, is then the highest that can be sampled by a trapped electron on that field line.

If one evaluates f_M, beginning the field line integration at various equatorial radii and azimuths, one can delineate the regions within which radiation above some predetermined frequency originates. Given a specific field model (e.g. O_4 or JPL), the possible source locations of the decameter radiation can be found as a function of frequency: higher frequencies coming from increasingly restricted areas and lower altitudes within the magnetosphere. In our calculations, we have found it sufficient to consider equatorial radii $L \leqslant 6$. Here, L denotes a magnetic field line that intersects the equatorial plane at $r/R_{\mathcal{U}} \equiv L$. The analysis can be readily extended to larger L-values, if desired. [The reader will note that L has been defined with respect to the zenographic, rather than the zenomagnetic, equator for computational convenience. Our analysis is insensitive to small changes in L that would result if we used the more customary definition.]

Figure 1 illustrates the results of such a calculation using the 0_4 model. Shown in a two-dimensional polar plot are the projections onto the surface of regions within which f_M exceeds 10, 16, 20 and 27 MHz in the northern hemisphere (Figure 1a), and southern hemisphere (Figure 1b). Only those regions accessible to electrons on L-shells of 2, 3, 4, 5, and 6 are indicated. Also plotted in the figure are the footprints at the cloud tops of those same L-shells. Finally, the figure includes contours of constant surface magnetic field intensity plotted in one-Gauss increments. The maximum gyrofrequency sampled by trapped electrons at altitudes above the Jovian cloud tops is found to be nearly 29 MHz – close to the maximum of the Io-independent DAM.

Several features on the plots are noteworthy. First, it is clear that f_M exceeds 27 MHz over a small region, very confined in azimuth, accessible to electrons on L-shells between three and six. In the northern hemisphere, the $f_M \geq 27$ MHz region occurs at lower latitudes than the corresponding region in the southern hemisphere. As the mirror point gyrofrequency decreases, larger emission regions become accessible. By 16 MHz, particles on the L = 6 flux tube can radiate from all azimuths. As the mirror point gyrofrequency reaches 10 MHz, electrons on L-shells ≥ 2 can radiate at all azimuths (except for a small region near $\lambda_{III} = 280°$). This is not to say, however, that radiation at these low frequencies should be observable from all CML. The detectability of the radiation depends critically, of course, on the excitation mechanism, beaming pattern, and on propagation effects such as refraction. Also, it is not known a priori which L-shells are populated with electrons that produce DAM. Although it is generally assumed that the Io-controlled component originates at L = 6 (the orbit of Io), no such general statement can be made about the component independent of Io control.

For comparison, in Figure 2, a similar plot has been constructed using the JPL model. As mentioned above, the most significant difference in this model is the location of the maximum southern hemisphere field at $\lambda_{III} = 330°$. As a consequence, the location of regions within which trapped electrons sample gyrofrequencies in excess of 27 MHz is now a very small area between L = 5-6, at higher λ_{III} than in the 0_4 model. Another difference between the models is that the highest surface field in the JPL model is greater than 15G, but is about 14G in the 0_4 model. [It should be noted that this model seems unique in this respect. The other Smith et al. (1976) models we have examined, as well as that of Smith et al. (1975), predict maximum fields of about 14G, but still systematically higher than those found in either the 0_4 model or the unpublished Acuña and Ness model 0_5, which contains the same number of coefficients as the JPL model that we are using.] It is also noteworthy that the highest gyrofrequency that can be sampled at all azimuths is 16 MHz in the 0_4 model and 20 MHz in the JPL model. This difference would also hold true for precipitating electrons.

b) Radiation Pattern

If, as we suppose, the decameter radiation is generated by an instability of an electron in gyroresonance with a wave having ω near ω_R, then the growth rate of such a wave will have a maximum in a direction determined by both plasma kinetic processes and by large-scale gradients in the local magnetic field. Regardless of the instability mechanism, there is evidence that the decameter radiation above 10 MHz is beamed into a conical surface with a fairly wide half-angle, Ψ (v. Dulk 1967, and Carr and Desch 1976) which is about 80° if L = 6 is the flux tube of the source.

Using either magnetic field models, it is possible to find the apparent source locations in CML from which radiation would be received in the ecliptic from the two sides of the emission cone. In general, the axis of the cone will be inclined to the equator by an angle ι, while the cone will intersect the equator along a curve whose asymptotes are two straight lines intersecting at an angle 2μ. Once μ is determined, the source locations are easily computed. From Goldreich and Lynden-Bell (1969), μ can be found from

$$\tan \mu = \sqrt{(\tan^2 \Psi \cos^2 \iota - \sin^2 \iota)} \qquad (3)$$

The angle ι is defined by $\iota = \cos^{-1} (B_e/B)$, where B_e is the projection of B onto the equator. If we describe the Jovian field temporarily in terms of a conventional right-handed spherical coordinate system in which ϕ is East Longitude, then B_e is given by

$$B_e = \sqrt{[B_\phi^2 + (B_r \sin\theta + B_\phi \cos\theta)^2]} \qquad (4)$$

Defining $\beta = \sin^{-1} (B_\phi/B_e)$, the System III longitude toward which $B_e(-B_e)$ points in the northern (southern) hemisphere is $\lambda_{III}' = \phi_{III} - \beta$. (Because System III is a West Longitude convention, $\phi_{III} \equiv 2\pi - \phi$). Finally, the apparent source locations seen from the equator, are $\Lambda_{III}(\pm\mu) \equiv \lambda_{III}' \pm \mu$, with plus and minus designating the two sides of the emission cone. The apparent source locations are thus seen to be rather sensitive functions of Ψ and ι.

Once the emission cone angle, Ψ, is chosen, the apparent source locations can be found for emission generated at any point on a magnetic flux tube. When ι is large, the emission cone may not intersect the ecliptic at all, while for small values of ι, the cone points nearly directly into the ecliptic, resulting in source locations separated by $2\mu \cong 2\Psi$.

Whether or not radiation at some frequency, f, will actually be observed in the ecliptic from a particular CML will depend on several factors. First, of course, f cannot

exceed f_M at the apex of the emission cone; and second, given Ψ, the emission cone must intersect the ecliptic, i.e. $\iota \leq \Psi$. But even these conditions may not suffice. The occurrence probability, P, of the various decameter sources appears to be a very sensitive function of ι. This has been inferred indirectly from the large variation of P with D_E. [D_E is the Jovicentric declination of the earth -- the angle of the Jupiter-Earth line with respect to the plane of Jupiter's equator, varying by $\pm$ 3.3° during a 11.9 year Jovian orbital period. We will return to a discussion of the Declination Effect below.] The evidence suggests that P is largest when the magnetic field in the emitting region is most inclined toward the earth (v., e.g. Dulk 1967, and Schatten and Ness 1971). We are thus led to the following assumption: along a given L-shell, the highest occurrence probabilities are located at minima in plots of ι versus Λ_{III}. Furthermore, there should be a qualitative resemblance between ι plotted against Λ_{III}, and plots of P versus CML.

A quantitative justification of this assumption must await a more detailed treatment (including refraction effects) of the emission mechanism. We now proceed to consider in some detail the variation in ι with CML, Ψ, L and hemisphere, and its relationship to observed DAM morphology.

c) Location and Occurrence Probability of the Io-Independent DAM

To find the regions of CML where radiation is most strongly beamed into the ecliptic (minima in a plot of ι versus Λ_{III}), it is necessary to choose Ψ. Dulk (1967), in analyzing the Io-related components, concluded that $\Psi \cong 79°$ would associate the Io-A and B (Main and Early) sources with two sides of a single emission cone. Goldreich and Lynden-Bell (1969) found support for this value from independent theoretical arguments. However, as there is no a priori reason for the non-Io-components to be generated by the

same mechanism, we treat Ψ for the moment as a free parameter. The angle will be chosen to give the observed separation between the non-Io A and B sources in the northern hemisphere. At 10 MHz we have found it necessary to choose a value for Ψ in the southern hemisphere which differs from the one that gives the best fit for the northern hemisphere sources.

Desch et al. (1975) and Desch (1976) have discussed the distinction between the Io-controlled and Io-independent sources at various frequencies. They noted that at any given frequency, the Io-independent radiation is less intense than the Io-controlled. Thus, for example, at 26.3 MHz, DAM noise storms having peak fluxes of less than 2×10^4 Jy ($1\ \text{Jy} = 10^{-26}\ \text{W m}^{-2}\ \text{Hz}^{-1}$) are predominantly independent of Io control. At that frequency, high occurrence probabilities are centered near 110° and 250° CML; non-Io B and A, respectively.

We begin our interpretive discussions at high frequencies (27 MHz) where the analysis is relatively simple, and then progress by stages to the more complicated situation at 10 MHz. A gyrofrequency of 27 MHz (and by implication, the apex of the emission cone) is found over only a very limited range of λ_{III} (cf. Figures 1 and 2). Thus the two sides of the emission cone will only intercept the ecliptic over a limited range of Λ_{III}.

When the O_4 model is used, the longitude range within which one can obtain f = 27 MHz in the northern hemisphere coincides with the greatest inclination of the emission cone toward the equator (i.e., ι attains its minimum values). In the south the conjugate longitude range occurs near the maximum values of ι. Hence, even before choosing a value for Ψ, it is clear that emission at 27 MHz will be most easily beamed into the equator from the northern hemisphere. This is encouraging because, as mentioned above,

studies of the Io-controlled sources have led to the conclusion that the source locations are correlated with small values of ι.

In choosing Ψ, it was natural to try first the value of 79° obtained by Dulk (1967). The results are shown in Figure 3, where ι is plotted against Λ_{III} for various L-values and for both hemispheres. Note that there is no curve for L = 2 because $f_M < 27$ MHz everywhere on that L-shell. The two symmetric curves ($\Lambda_{III} = \lambda'_{III} \pm \mu$) stand out clearly. Because ι in the southern hemisphere is large, radiation from there would not easily reach the ecliptic; nor is there observational evidence for left-polarized radiation at 27 MHz. (Electromagnetic waves propagating in the R-X mode would be received at Earth as right-polarized if emitted from the northern hemisphere and left-polarized if emitted from the south.) In the northern hemisphere, with $\Psi = 79°$, the two sides of the emission cone along L = 6 intercept the equator at Λ_{III} centered near 120° and 270°. This corresponds closely to the observed locations of non-Io B and A, respectively. When L-values less than six are considered $\Psi \cong 60°$ fits somewhat better. In general, it will not be possible to use this beaming model to determine the L-shell on which Io-independent radiation originates.

Thus, with $\Psi = 79°$ (or 60° for $L < 6$), minima in ι are located where Λ_{III} equals the observed CML of the non-Io A and B sources. However, as expected, the resemblance of Figure 3 to observations of occurrence probability is only qualitative. In particular, the observed occurrence probabilities of Sources A and B are never equal, and generally non-Io A occurs more frequently than non-Io B. Whether this asymmetry may be a consequence of refraction is a question to which we return below.

A similar plot can be constructed using the JPL model. However, at 27 MHz, only L values of 5 and 6 allow $f_M \geq 27$ MHz, and then only over a very narrow range of longitudes (cf. Figure 2). In fact, $\iota \geq 50°$ in both hemispheres. Thus, in this model and at this frequency, radiation is not readily beamed into the ecliptic at any longitude.

In general, as f_M is decreased and as the altitude of the source region increases, the differences between the O_4 and JPL models become smaller, disappearing altogether by 10 MHz. These discrepancies probably result from the large extrapolation of the Pioneer 11 data from the region where they were obtained to the very low altitudes at which $f_M \gtrsim 20$ MHz. Gyrofrequencies of 27 MHz are found only close to the cloud tops, and the octupole contributions, which are the least well-determined, are very important, while lower gyrofrequencies (~10 MHz), are found at considerably higher altitudes where the extrapolations of the Pioneer 11 data are not as severe. Thus it is not surprising that the magnetic field models tend to become similar at lower frequencies. One should also keep in mind that 27 MHz is very close to the observed upper limit of the non-Io DAM. Io-independent radiation is clearly present at 26.3 MHz (Desch et al. 1975), and has probably been seen at 27.6 MHz (Thieman and Smith 1978), but thus far no definitive identifications have been made at higher frequencies (v. Wilson, Warwick, and Libby 1968).

At 20 MHz, $\Psi = 79°$ again appears to locate the minima in ι versus Λ_{III} closer to the observed source locations of non-Io A and B, than does, say $\Psi = 60°$, at least for radiation originating near $L \cong 5$-6. In Figure 4, the computed values of ι are shown using the O_4 model. For clarity, northern and southern hemispheres are plotted separately. In the northern hemisphere, broad minima in ι occur near $\Lambda_{III} \cong 80°$–$150°$ and $240°$–$330°$ at $L \cong 6$. Lower values of ι occur at lower L-values, again suggesting the possibility that

the non-Io DAM may originate inside a large region of the magnetosphere bounded by L between 2 and 6. If the radiation is dominated by sources at low L-values, then $\Psi \cong 60°$ provides a better fit for the location of non-Io A and B. There is no way to distinguish between these two possibilities within the context of this model.

In the southern hemisphere, narrow minima in ι occur near $\Lambda_{III} \cong 15°$ and 160°. The narrowness of these minima suggests that it might be comparatively difficult for radiation excited in the southern hemisphere to reach the ecliptic plane. From L = 6 there is an additional area of small ι near $\Lambda_{III} \cong 90°$ and 300°.

The works of Desch (1976), Bozyan and Douglas (1976), and Thieman (1977) contain extensive analyses of DAM observations at 18 or 20 MHz. The non-Io controlled components are most likely to be observed near 160° CML (non-Io B), 250° CML (non-Io A) and 320° CML (non-Io C or Late Source). As before, the Early and Main Sources (B and A) have a natural explanation in terms of this beaming model. In addition, based on the 0_4 model, the radiation from Source C may also originate in the northern hemisphere, because small values of ι extend to 330° on the L = 6 plot. However, Kennedy (1969) has reported that Source C is often left-circularly polarized, which suggests that it originates in the southern hemisphere. The southern hemisphere minimum on L = 6 at 300° in Figure 4b is close to Source C, while the second minimum near 90° could be an indication of an Io-independent Source D.

Support for the idea that Source C comes from the southern hemisphere can be found from the JPL model (Figure 5). The northern hemisphere minima in ι (Figure 5a) are similar, though narrower than those in Figure 4a. In particular, for the region near $\Lambda_{III} \cong 240°$, the minimum in ι no longer extends into the Source C region. [Also note

that $f_M < 20$ MHz virtually everywhere on L = 2.] In this model, the southern hemisphere ι minima are found near $\Lambda_{III} \cong 130°$ and 330°. Emission beamed from 130° CML in the southern hemisphere could be masked by emission from the same CML in the north. Emission beamed from the minimum in ι at $\Lambda_{III} \cong 330°$ in Figure 5b is within the observed non-Io C source. It is also interesting to note that non-Io C is not observed above 22 MHz; and in neither of the magnetic field models is there any possibility of beaming into the ecliptic from that source region in either hemisphere at 27 MHz. In fact, there is a general tendency in the southern hemisphere for the highest frequency source regions ($f_M > 20$ MHz) to be located where ι is large (cf. Figure 3). In contrast, in the north the highest frequency source regions are located where ι is small.

The two multipole magnetic field models both suggest an enhanced probability that radiation emitted into a 79° (L ≅ 6) or 60° (L ≅ 3) emission cone angle will be seen in the ecliptic as coming from the observed source locations of non-Io A and B. Concerning Source C, the information provided by these models is ambiguous. Taken together, they argue for non-Io C coming from the southern hemisphere, with some contribution from an extended Source A in the northern hemisphere. However, while this geometrical construction provides a clear framework within which the northern hemisphere sources can be understood, the location of Source C is not as well determined. The reasons for this asymmetry are considered in detail in the accompanying paper by Goldstein and Eviatar (1978), but we will mention one difficulty here. Because there are so many similarities between the Io-controlled and Io-independent DAM sources, it is natural to assume that regardless of the specific excitation mechanism, the source locations should be closely related. The Io-C source is observed when the phase of Io is near 240° as measured from

superior geocentric conjunction. This places the Io-C source on the $+\mu$ side of the emission cone. However, in both field models the small values of ι in the southern hemisphere are found near $\lambda_{III} = 50°$, thus placing the non-Io C beaming pattern on the $-\mu$ side of the cone. No more can be said about this in the present context, and further discussion will be deferred to the companion paper.

At 16 MHz, both the observed source morphology and plots of ι versus Λ_{III} are qualitatively the same as at 20 MHz.

Before describing the beaming model at 10 MHz, we should review the following observations. The observed source locations have shifted noticeably at 10 MHz. This shift has been investigated in some detail by Thieman and Smith (1978), who suggest that between 15 and 10 MHz, Sources A and B have gradually moved together, merging by 10 MHz into a single source at 210° CML. Between 22 and 10 MHz the position of Source C increases linearly, reaching a CML of about 350° at 10 MHz. The Fourth Source, D, near 60° CML becomes apparent below 18 MHz, though Io-independent radiation from that source has not been observed.

The theoretical situation at 10 MHz is also more complicated than at higher frequencies. To fit the model to the observation that there is a single source at $\Lambda_{III} \cong 200°$, some change in Ψ is necessary. The minimum value of Ψ that still results in emission into the ecliptic from $L \lesssim 6$ is $\Psi \cong 40°$. Emission from the northern hemisphere from $L \cong 5$–6 is then concentrated around $\Lambda_{III} \cong 200°$ (Figure 6a). [Note that at 10 MHz, the 0_4 and JPL models are essentially identical in all respects in both hemispheres.] With $\Psi \cong 40°$, however, the emission cone in the southern hemisphere barely intersects the ecliptic at all at $L \cong 6$. It is possible that very little emission from a 40° cone could

be beamed into the ecliptic. But if emission from the south were beamed into a cone with $\Psi \cong 60°$ (Figure 6b), then the preferred directions (small ι) would be $\Lambda_{III} \cong 110°$ and 360°, close to positions of Io-D and non-Io C, respectively. One implication of this scenario at 10 MHz is that whatever the emission mechanism, more intense radiation should be produced as Ψ decreases from 79° to 40°, at least at low frequencies. Or, alternatively, radiation emitted locally at relatively large Ψ and low frequency is focused by refraction into a smaller emission cone as the radiation leaves the Jovian environment. (At high frequencies -- 20 MHz and above, Figures 4 and 5 -- emission from L = 6 cannot intercept the ecliptic from either hemisphere if Ψ is as small as 40°.)

If one takes $L \lesssim 3$ as the appropriate source location of the Io-independent DAM, then $\Psi \cong 20°$ would be necessary to produce a minimum in ι at Λ_{III} between 170°–230° from the north, but $\Psi \cong 60°$ would still suffice in the south. Furthermore, radiation from $L \cong 2$ is beamed almost directly into the ecliptic, and should show little, if any, dependence on CML. In fact, although the occurrence probability of the Io-independent DAM (peak flux $\leqslant 4 \times 10^6$ Jy; Desch 1976) is modulated in CML, there remains nearly a 50% occurrence probability of detecting radiation at any CML (v. Dulk and Clark 1966 and Thieman 1977). This illustrates a systematic trend that is supported by these geometrical constructions; viz., that while the minima in ι as a function of Λ_{III} indicate regions of preferred beaming into the ecliptic, as ι decreases with decreasing frequency for a given L-value, an increasing fraction of the emission should become independent of CML.

d) The Declination Effect

It has been known for some time that the longitude of the center of Source A is closely correlated with D_E (v. Carr and Gulkis 1969, and Carr and Desch 1976, for reviews).

This sinusoidal drift of Source A is thought to occur only in the non-Io controlled source (Register and Smith 1969, Goertz 1971). The variation with D_E is not a simple shift of the center of the occurrence probability pattern, but is rather more intricate. Source A emission usually begins at the same CML (200°) independent of D_E. However, as D_E becomes more positive, the high longitude boundary of Source A moves from 280° CML to higher longitudes, reaching 320° CML when $D_E = +3.3°$, a change of some 40°. The centroid of the source also drifts, but by a lesser amount ($\cong$ 15°) (Bozyan and Douglas 1976). Although Donivan and Carr (1969) have reported finding a weaker shift of the Source B centroid that was in phase with the Source A drift, Thieman (1977) found only a hint of an in phase drift for non-Io B, which may not have been statistically significant.

The geometrical beaming model we have proposed for the locations of the various non-Io sources can also explain this variation in Sources A and B with D_E. One of the effects of varying D_E is intuitively obvious, though unimportant as we shall see. As D_E increases, the two sides of the emission cone that intersect the ecliptic will tend to move apart; i.e., 2μ will tend to increase, producing an anti-phase variation in the centroids of Sources A and B, contrary to observation. That this is actually a very small effect, an order of magnitude smaller than the observed 40° expansion in Source A, can be seen by noting that the centroids of non-Io A and B at, say, 20 MHz, are separated by some 140°, while the maximum allowed separation, assuming a 79° emission cone, is 158°. The change in 2μ is actually much less than this maximum of 20°, for D_E changes by at most 6.6° and so the maximum cannot be reached. With $\iota \cong 45°$ (cf. Figures 5a and 6a) and using equation (3), the variation in 2μ is found to be of order 5°. The variation is even smaller if the radiation originates at lower L-values.

There is, however, another explanation. For the sake of this exposition, assume that non-Io DAM originates at L = 6, that the JPL model gives the appropriate variation of ι with CML at 20 MHz, and $\Psi = 79°$. [This argument can be modified to utilize the 0_4 model and/or a source location inside L = 6.] When $D_E = -3.3°$, the extent of non-Io A is some 80°. In Figure 7, part of the L = 6 curve from Figure 5a is redrawn. A line, denoted $D_E = -3.3°$, at $\iota \cong 44°$ intersects the Source A region at points (a) and (b) separated by 80°. Assume that above the line, radiation is received in the ecliptic, but radiation emitted below the line with larger ι is not. When D_E is increased to +3.3°, a second line can be drawn at $\iota \cong 50°$, which intersects the Source A region at points (c) and (d). The high longitude boundary of Source A has moved some 50°, while the beginning of Source A has moved at most by 25° (probably less because of potential interference from Source B). Furthermore, the longitudes of the Source A and B centroids will increase in phase.

This argument is only meant to be suggestive. Our present knowledge of the near-surface Jovian magnetic field is too imprecise for more detailed modeling. Furthermore, refraction and other propagation effects are likely to play an important role in any complete explanation of this phenomenon. However, several general features are germane. First, the fact that the high longitude boundaries of Sources A and B may move in phase by as much as 40° does not necessarily contradict predictions based on Dulk's (1967) conical sheet model, since the motion proposed here is not caused by a tilting of the cone axis. Second, there is ample reason to expect that inhomogeneities in the near surface Jovian fields will produce the very asymmetrical drifts of the low and high longitude sides of Source A that are observed, and that we have described at least qualitatively in terms of this beaming model. Two caveats should be noted. One is that we cannot estimate how much the centroids of non-Io A and B will drift, except to say that for non-Io

A it should be more than the 5° that results from the change in 2μ discussed above, or non-Io B, the drift due to changes in 2μ will tend to cancel the change in the centroid produced by the asymmetrical expansion of B to higher longitudes. The expected result is that the drift of the centroid of B will be less than that of A, as observed. The second is that, although this construction implies that the low longitude side of A (and B) should drift much less than, and in a direction opposite to, the high longitude side, there is no observational evidence to suggest that the low longitude side of Source A (or B) drifts at all.

III. CONCLUSIONS

The theoretical model we have presented is, we believe, useful for explaining some of the significant features of the Io-independent Jovian decameter radiation.

It is based on four assumptions, which hopefully will be tested experimentally on future space probes to Jupiter. The first of these is that the Io-independent DAM is produced by electrons stably trapped in Jupiter's inner magnetosphere ($L \lesssim 6$); second, that the radiation is excited near the local gyrofrequency in the R-X mode; third, that the radiation is beamed into a conical surface; and last, that the beaming of radiation into the ecliptic depends sensitively on the magnitude of the tilt of the emission cone toward the Jovian equatorial plane.

The first two assumptions imply that the Io-independent sources radiate below 29 MHz, for only precipitating particles can reach higher gyrofrequencies. Thus we do not expect Io-independent radiation to be seen much above 29 MHz.

Above 10 MHz, this model suggests that decameter radiation is beamed into a conical surface with a half-angle, Ψ, that is between 60°–80°. The lower value obtains if radiation originates at small L-values ($L \gtrsim 3$), while emission near $L \cong 6$ requires $\Psi \cong 80°$. At 10 MHz, it was necessary to choose Ψ independently in the two hemispheres – 40° in the north, and 60° in the south.

The model constructed is then consistent with several features of DAM morphology. The association of low values of ι with high occurrence probabilities leads to the conclusion that at 27 MHz, radiation is preferentially beamed into the ecliptic from only the northern hemisphere, and only at the central meridian longitudes of the non-Io A and B sources. Below 27 MHz, two additional regions of small ι become apparent, originating

in the southern hemisphere. One of these lies near the location of non-Io C. But, as mentioned above, there are difficulties with this interpretation.

At 10 MHz, with suitable variation in Ψ, the beaming pattern shifts so that there is a single source from the northern hemisphere, near the observed location (200° CML), while two sources remain in the south, one of which may correspond to non-Io C. Because of the generally low values of ι at all longitudes, the model is consistent with the observed tendency at low frequencies for there to be considerable DAM noise independent of CML.

An additional success of the model is the suggested explanation of the large drift of the high longitude boundary of non-Io A with changes in D_E.

The model also suggests the possible existence of DAM features that have not yet been observed. These include a second southern hemisphere (left-circularly polarized) source near 150° CML ($f > 10$ MHz), as well as Io-independent emission from 120° CML (Source D) at 10 MHz. Because of the sensitivity of the beaming pattern to small changes in ι, it is also expected that when Jupiter is observed by space probes at high northern and/or southern latitudes, two trends will appear. One is an increased occurrence probability at high frequencies ($f \cong 27$ MHz) that is still strongly modulated with longitude. This is expected, because although one will be well inside the emission cone as it intercepts the receiver, the restricted azimuthal region within which, say, $f_M \geq 27$ MHz will continue to produce a strong modulation with longitude. The second effect, most noticeable as the frequency decreases below 16 MHz, would be a decline in the modulation of P with CML as the emitting region gradually expands to encompass nearly all longitudes.

One limitation of this geometrical model is the absence of an explanation for the significant differences in occurrence probability among the various Io-independent sources. For example, non-Io A generally has a higher occurrence probability than non-Io B (Carr and Desch 1976). The explanation for these differences may well depend on exactly how the inhomogeneities in the local magnetic fields affect both the amplification and propagation of the radiation in the source region. In general, these strong gradients in the near surface magnetic fields, where the high order multipole terms are very important, will not be symmetric about the emission cone. This is suggested by even cursory examination of Figures 1 and 2, and can be confirmed by more detailed calculations using either magnetic field model. Similarly, the effects of these gradients in the magnetic field on an electromagnetic wave propagating through this underdense plasma ($\omega_{pe} \ll |\Omega_e|$) should exceed the effects of any gradients in the density at these altitudes. Thus, refraction will tend to bend the wave number vector, $\underset{\sim}{k}$, toward the direction of $-\partial \ell nB/\partial \underset{\sim}{r}$ (Stix 1962, Smith 1973).

The maximum gradient in $\underset{\sim}{B}$ at these low altitudes lies close to the direction of $\underset{\sim}{B}$ itself. Consequently, a ray initially launched at $\Psi \cong 80°$ will be bent toward the axis of the emission cone. Unless ι is small (just how small is difficult to estimate without doing a complete ray-tracing calculation, which is beyond the scope of this paper), refraction toward the cone axis will have the effect of diminishing the amount of radiation that is beamed into the ecliptic. Because the gradients in $\underset{\sim}{B}$ are asymmetric about the emission cone axis, the amount of radiation beamed into the ecliptic should differ on the two sides of the cone, at least partially accounting for the differing occurrence probabilities of the various sources.

In the accompanying paper, the features of this geometrical model are combined with a specific instability mechanism in an attempt to reduce the number of assumptions needed to describe the Io-independent DAM. That analysis retains the assumption of excitation of DAM by trapped electrons. It is then found that the value of Ψ and the cone thickness, $\Delta\Psi$, can be determined as a function of frequency, and that the L-shell of the source region can be localized within some fairly well defined limits. The theory is also able to account for the excellent correlation in the northern hemisphere between small values of ι and the source locations. A solution to the difficulties encountered in explaining the geometry of the southern hemisphere source is also suggested, in which both the Io and non-Io C sources are emitted into the $+\mu$ side of the emission cone.

The authors would like to acknowledge the continued encouragement of Mr. Joseph Alexander, and Dr. Norman Ness. Drs. Mario Acuña, Keith Ogilvie, Leonard Burlaga, and Juan Roederer are thanked for their assistance and comments. The help of Messrs. Michael Kaiser and Richard Thompson with the numerical analysis is deeply appreciated. One of us (A.E.) would like to acknowledge the support provided by the Department of Physics and Astronomy of the University of Maryland and the Laboratory for Extraterrestrial Physics of the Goddard Space Flight Center during the summer of 1977, when this work was begun.

REFERENCES

Acuña, M. H., and Ness, N. F. 1976, in Jupiter, ed. T. Gehrels (Tucson: University of Arizona Press), 830.

Anderson, J. D., Null, G. W. and Wong, S. K. 1974, J. Geophys. Res., 79, 3661.

Atreya, S. K., and Donahue, T. M. 1976, in Jupiter, loc. cit. 304.

Bozyan, F. A., and Douglas, J. N. 1976, J. Geophys. Res., 81, 3387.

Carr, T. D., and Desch, M. D. 1976, in Jupiter, loc. cit., 693.

Carr, T. D., and Gulkis, S. 1969, Ann. Rev. Astron. Ap., 7, 577.

Desch, M. D. 1976, Ph. D. Thesis, University of Florida, Gainsville, Florida.

Desch, M. D., Carr, T. D., and Levy, J. 1975, Icarus, 25, 12.

Donivan, F. F., and Carr, T. D. 1969, Ap. J., 157, L65.

Dulk, G. A. 1967, Icarus, 7, 173.

Dulk, G. A. and Clark, T. A. 1966, Ap. J., 145, 945.

Fjeldbo, G., Kliore, A., Seidel, B., Sweetnam, D., and Woiceshyn, P. 1976, in Jupiter, loc. cit., 238.

Goertz, C. K. 1971, Nature, 229, 151.

Goldreich, P., and Lynden-Bell, D. 1969, Ap. J., 156, 59.

Goldstein, M. L., and Eviatar, A. 1972, Ap. J., 175, 275.

Goldstein, M. L., and Eviatar, A. 1978, preprint

Kahle, A. B., Kern, J. W. and Vestine, E. H. 1964, J. Geomag. and Geoelec., 16, 229.

Kennedy, D. J. 1969, Ph. D. Thesis, University of Florida, Gainsville, Florida.

Register, H. I., and Smith, A. G. 1969, Ap. Letters, 3, 209.

Schatten, K. H., and Ness, N. F. 1971, Ap. J., 165, 621.

Smith, E. J., Davis, Jr., L., and Jones, D. E. 1976, in Jupiter, loc. cit., 788.

Smith, E. J., Davis, Jr., L., Jones, D. E., Coleman, Jr., P. J., Colburn, D. S., Dyal, P., and Sonett, C. P. 1975, Science, 188, 451.

Smith, R. A. 1973, Ph. D. Thesis, University of Maryland, College Park, Maryland.

Stix, T. H. 1962, The Theory of Plasma Waves (New York: McGraw Hill).

Thieman, J. R. 1977, Ph. D. Thesis, University of Florida, Gainsville, Florida.

Thieman, J. R. and Smith, A. G. 1978, preprint.

Warwick, J. W. 1964, Ann. Rev. Astron. Ap., 2, 1.

Wilson, R. G., Warwick, J. W., and Libby, W. F. 1968, Nature, 220, 1215.

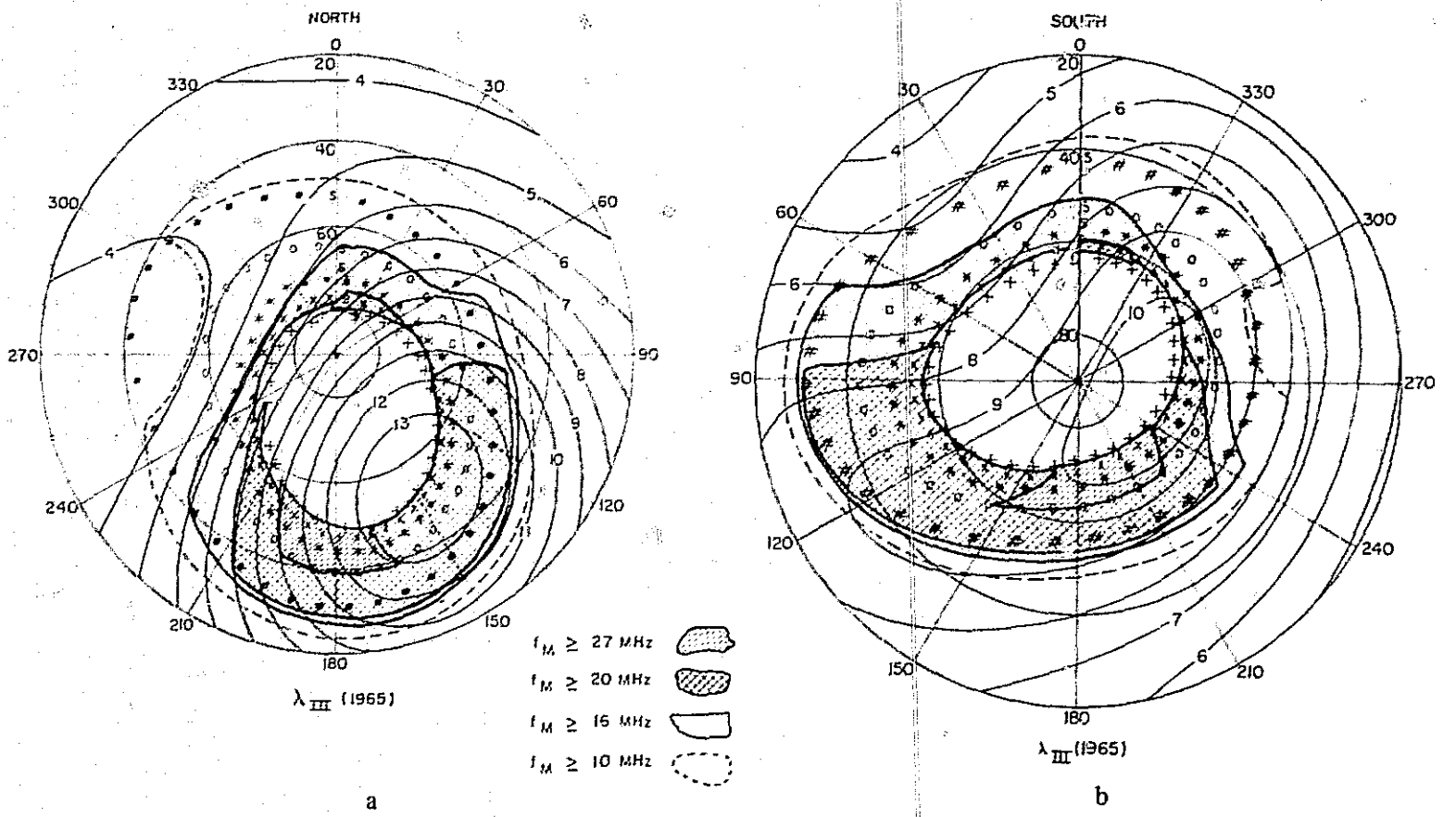

Figure 1. Two dimensional contour plots showing regions within which, f_M, the maximum electron gyrofrequency at the mirror field B_M, exceeds 27, 20, 16 or 10 MHz (shaded areas and dashed line). The contours are projected onto the altitude of the cloud tops. Also drawn are isointensity contours in 1G increments of Jupiter's surface field. Footprints on the surface are plotted for L = 6 ("+"), L = 5 ("X"), L = 4 ("*"), L = 3 ("0") and L = 2 ("#") field lines. The azimuthal spacing of the field lines in the equatorial plane is 10°. Conjugate points at any longitude can be found by noting that in the two hemispheres, near $\lambda_{III} = 0°$, footprints denoted "S" are conjugate. (0_4 model).

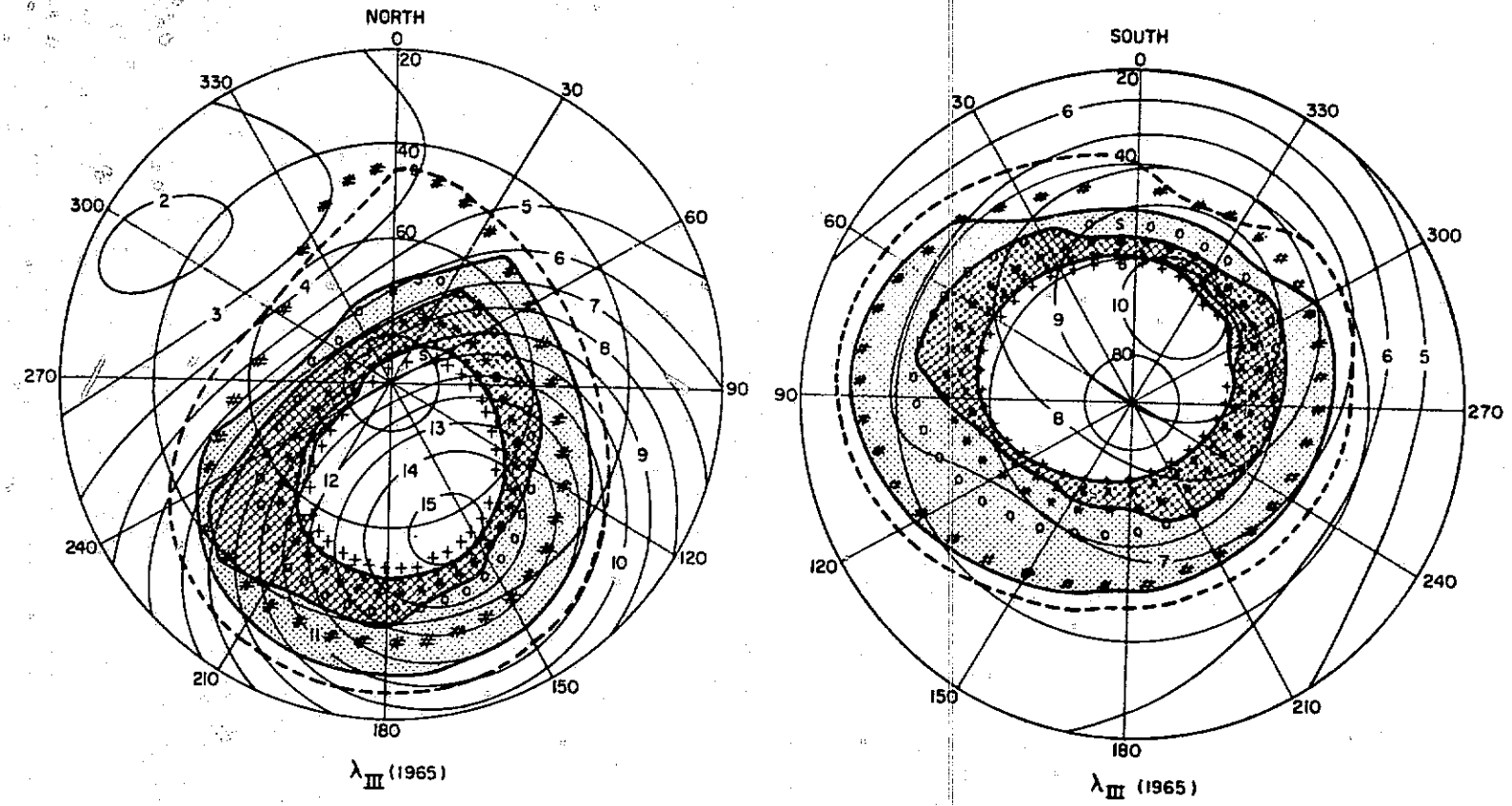

Figure 2. Similar to Figure 1, but using the JPL model.

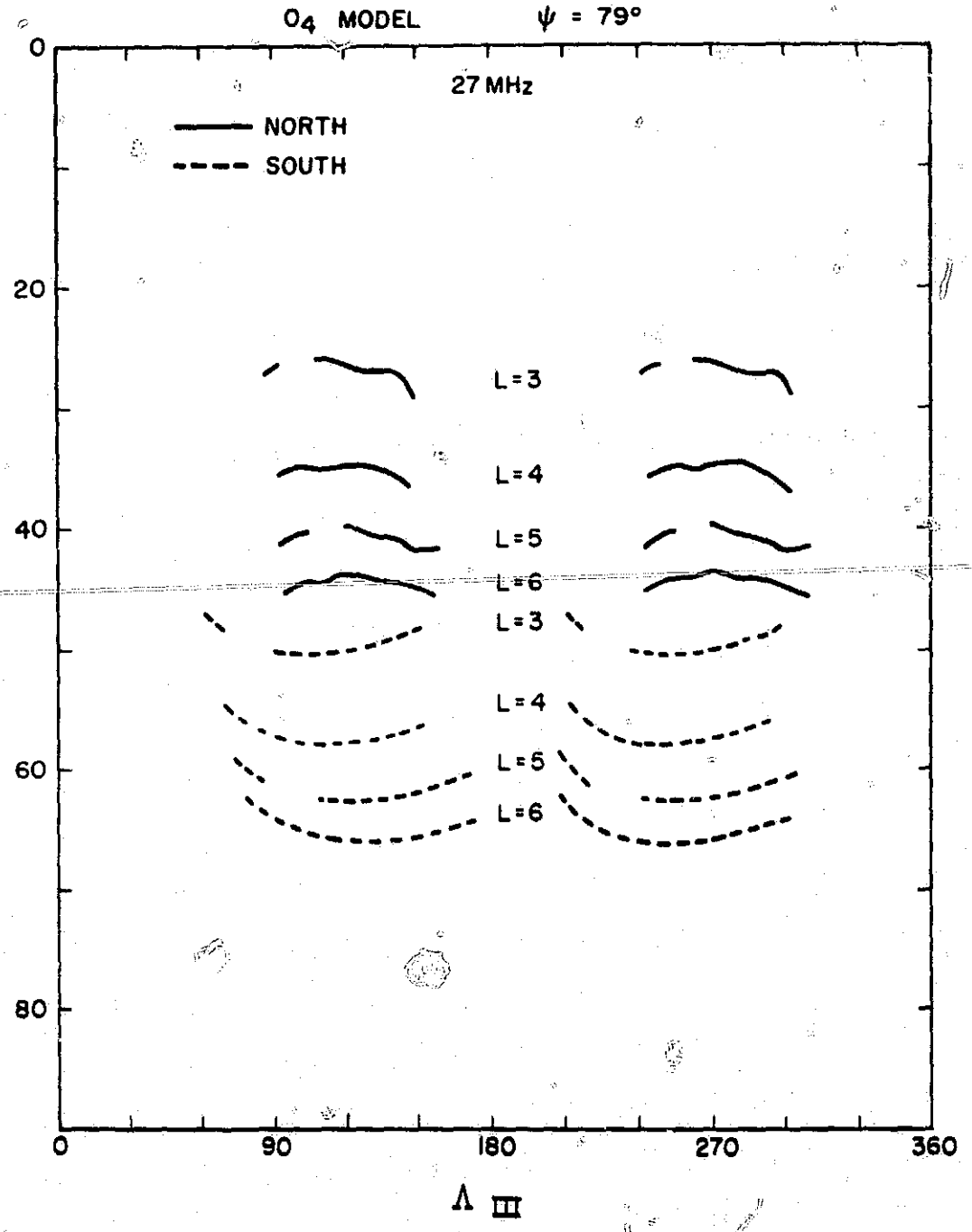

Figure 3. A plot of ι versus Λ_{III} at 27 MHz, using the 0_4 model with $\Psi = 79°$. Gaps in the curves for L = 3 and 5 result from localized regions where f_M is less than 27 MHz. Curves on the right are solutions of $\Lambda_{III} = \lambda_{III}' + \mu$ while those to the left are obtained from $\Lambda_{III} = \lambda_{III}' - \mu$. The curves represent the central meridian longitude directions of the intersection lines of the emission cone with the ecliptic. Note that there is no longitude for L = 2 at which $f_M \geq 27$ MHz (cf. Figure 1). Preferential beaming into the ecliptic – small values of ι – occurs at the positions of the Io independent Early and Main Sources (B and A, respectively).

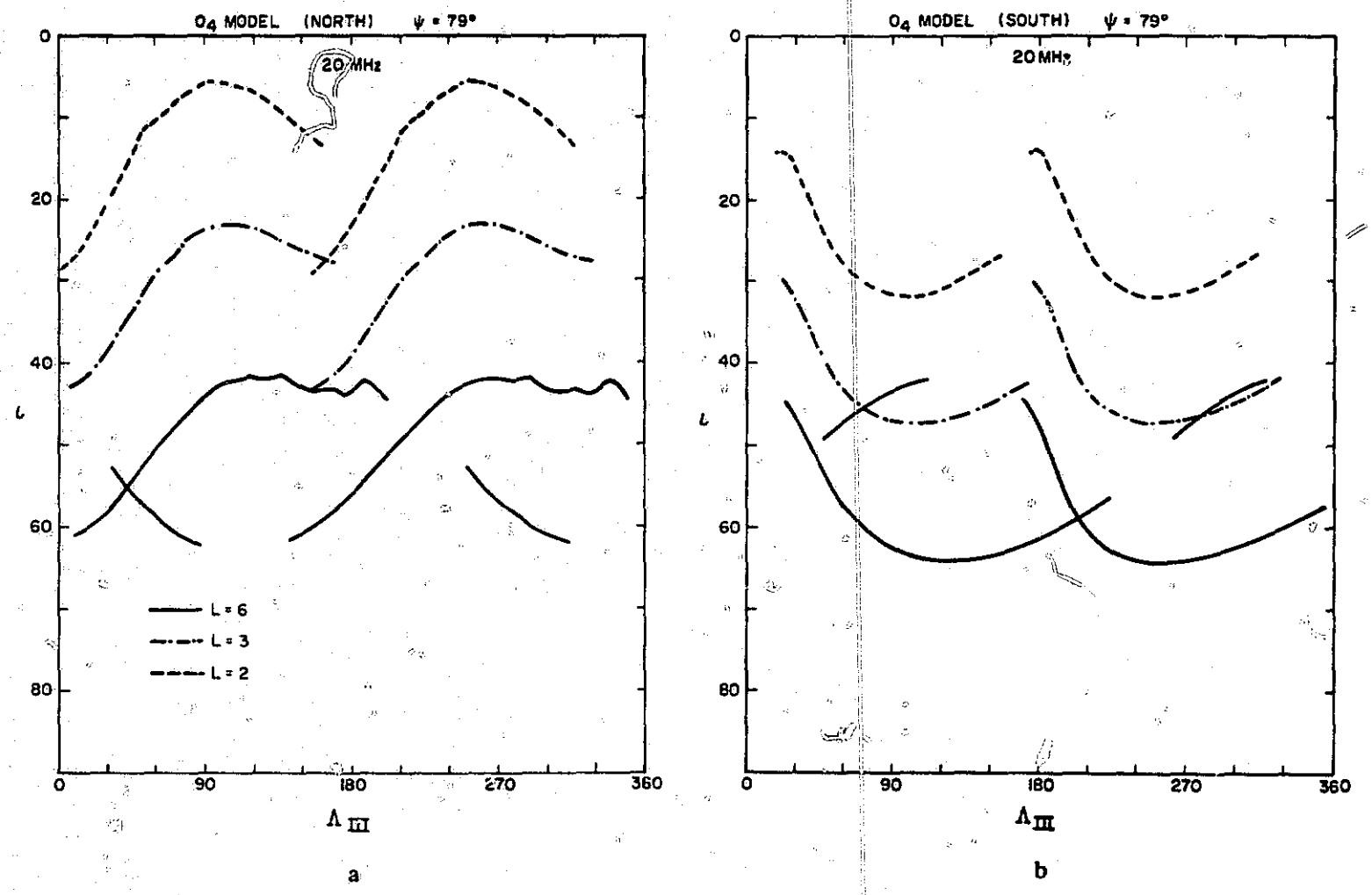

Figure 4. Similar to Figure 3, but for 20 MHz. For clarity, curves are not plotted for L = 4 or 5; and, northern and southern hemispheres are plotted separately (Figure 4a and 4b, respectively). In the north, minima in ι (peaks on the curves), occur near the CML of the non-Io A and B sources. Note that at L = 6, the preferred emission region for non-Io A extends to Third Source (C) longitudes. See the text for a discussion of the southern hemisphere sources.

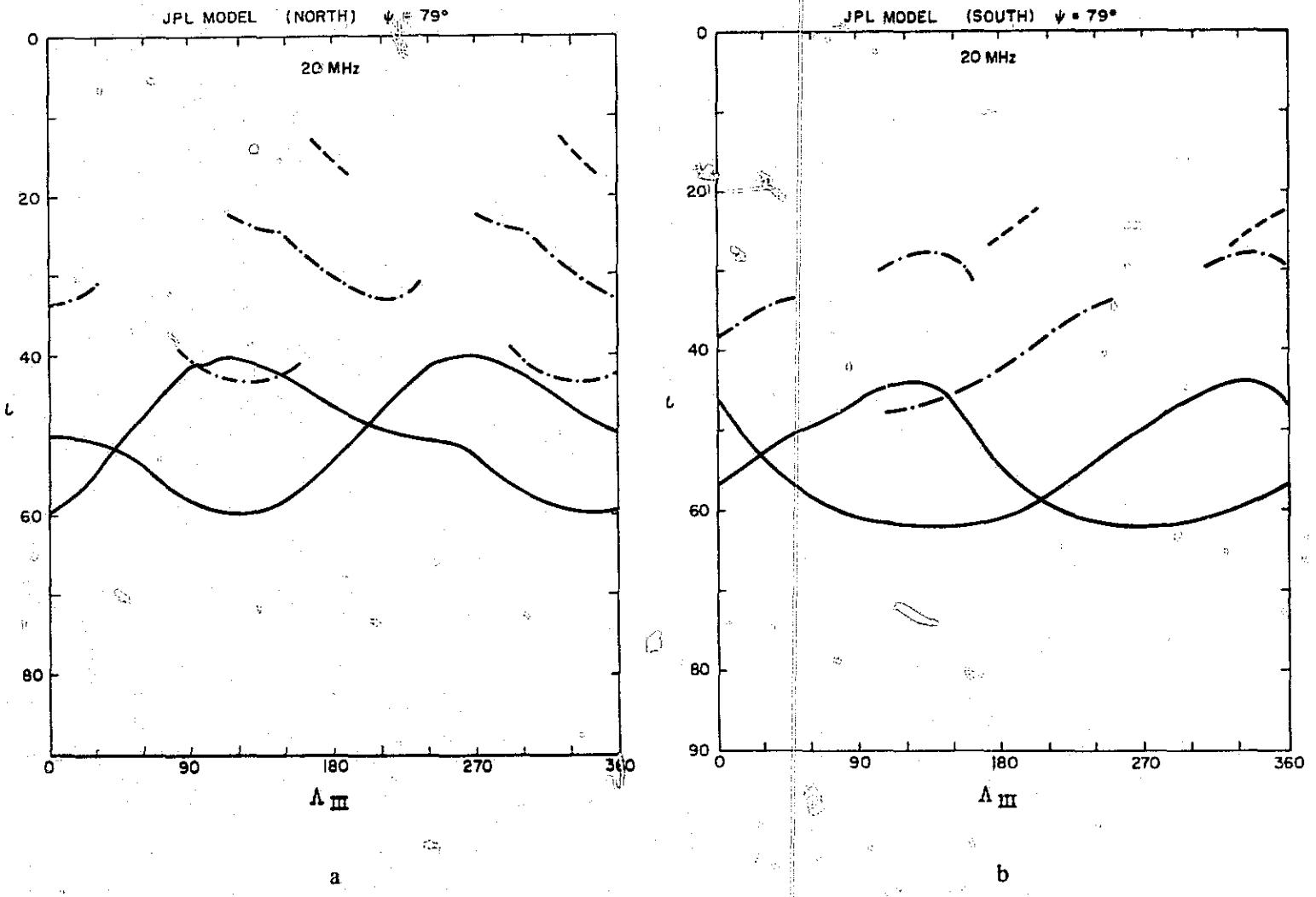

Figure 5. Similar to Figure 4, but using the JPL model. Note that for L = 2, the allowed range of Λ_{III} is much less than it was using the O_4 model (cf. Figure 3). In addition, at L = 6 in the north (Figure 5a), small values of ι do not extend to non-Io C longitudes. See the text for a discussion of the southern hemisphere source locations (Figure 5b).

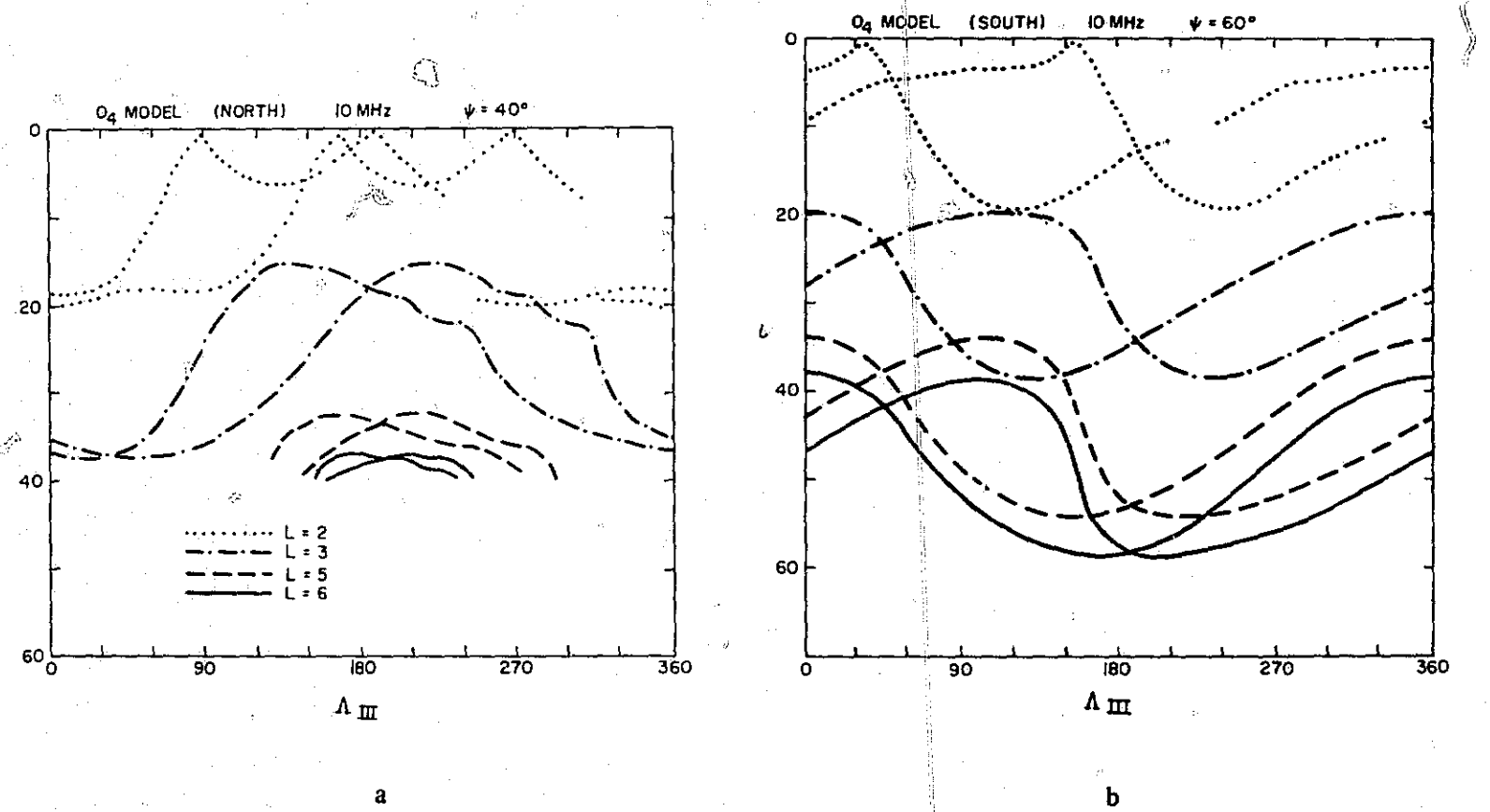

Figure 6. A plot of ι versus Λ_{III} at 10 MHz, using the 0_4 model. Use of the JPL model produces identical curves. In the north (Figure 6a) $\Psi = 40°$, in the south (Figure 6b) $\Psi = 60°$. See the text for a discussion of the source locations.

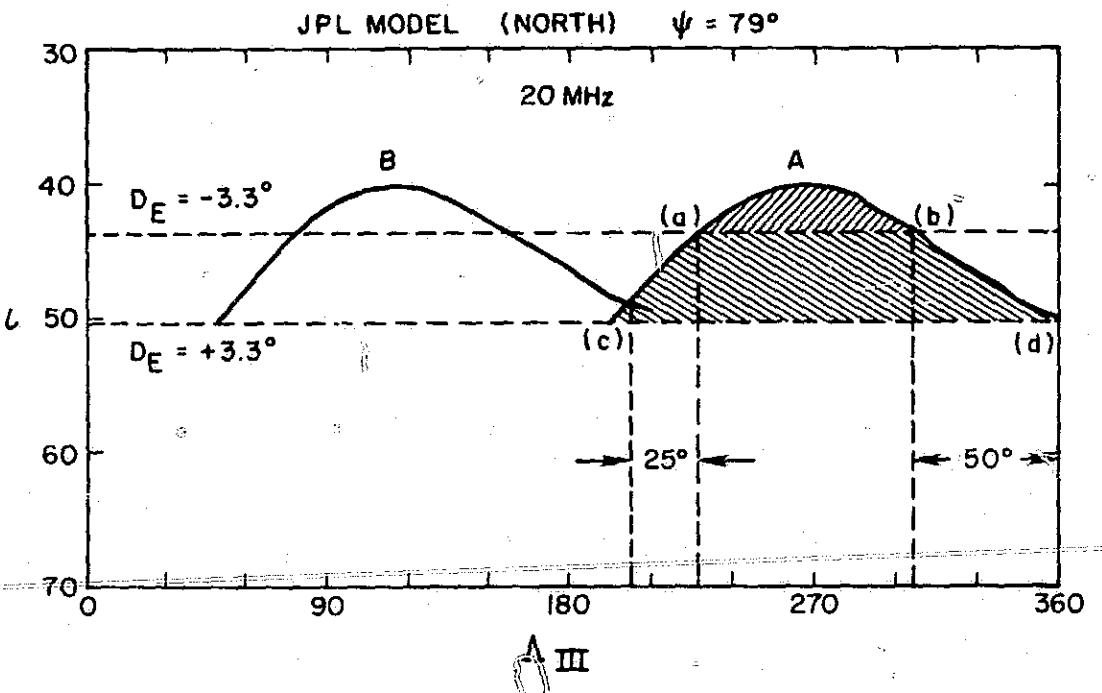

Figure 7. A possible explanation of the Declination Effect is shown. As D_E changes from -3.3° to +3.3°, the width of non-Io A can increase from $\Delta\Lambda_{III}$ = (b) – (a) to $\Delta\Lambda_{III}$ = (d) – (c). (JPL model on L = 6, northern hemisphere).

FIGURE CAPTIONS

Figure 1. Two dimensional contour plots showing regions within which, f_M, the maximum electron gyrofrequency at the mirror field B_M, exceeds 27, 20, 16 or 10 MHz (shaded areas and dashed line). The contours are projected onto the altitude of the cloud tops. Also drawn are isointensity contours in 1G increments of Jupiter's surface field. Footprints on the surface are plotted for L = 6 ("+"), L = 5 ("X"), L = 4 ("*"), L = 3 ("0") and L = 2 ("#") field lines. The azimuthal spacing of the field lines in the equatorial plane is 10°. Conjugate points at any longitude can be found by noting that in the two hemispheres, near $\lambda_{III} = 0°$, footprints denoted "S" are conjugate. (0_4 model).

Figure 2. Similar to Figure 1, but using the JPL model.

Figure 3. A plot of ι versus Λ_{III} at 27 MHz, using the 0_4 model with $\Psi = 79°$. Gaps in the curves for L = 3 and 5 result from localized regions where f_M is less than 27 MHz. Curves on the right are solutions of $\Lambda_{III} = \lambda_{III}' + \mu$, while those to the left are obtained from $\Lambda_{III} = \lambda_{III}' - \mu$. The curves represent the central meridian longitude directions of the intersection lines of the emission cone with the ecliptic. Note that there is no longitude for L = 2 at which $f_M \geq 27$ MHz (cf. Figure 1). Preferential beaming into the ecliptic – small values of ι – occurs at the positions of the Io independent Early and Main Sources (B and A, respectively).

Figure 4. Similar to Figure 3, but for 20 MHz. For clarity, curves are not plotted for L = 4 or 5; and, northern and southern hemispheres are plotted separately (Figures 4a and 4b, respectively). In the north, minima in ι (peaks on the curves), occur near the CML of the non-Io A and B sources. Note that at L = 6, the preferred emission region

for non-Io A extends to Third Source (C) longitudes. See the text for a discussion of the southern hemisphere sources.

Figure 5. Similar to Figure 4, but using the JPL model. Note that for L = 2, the allowed range of Λ_{III} is much less than it was using the O_4 model (cf. Figure 3). In addition, at L = 6 in the north (Figure 5a), small values of ι do not extend to non-Io C longitudes. See the text for a discussion of the southern hemisphere source locations (Figure 5b).

Figure 6. A plot of ι versus Λ_{III} at 10 MHz, using the O_4 model, Use of the JPL model produces identical curves. In the north (Figure 6a) $\Psi = 40°$, in the south (Figure 6b) $\Psi = 60°$. See the text for a discussion of the source locations.

Figure 7. A possible explanation of the Declination Effect is shown. As D_E changes from $-3.3°$ to $+3.3°$, the width of non-Io A can increase from $\Delta\Lambda_{III}$ = (b) – (a) to $\Delta\Lambda_{III}$ = (d) – (c). (JPL model on L = 6, northern hemisphere).

BIBLIOGRAPHIC DATA SHEET

1. Report No.	2. Government Accession No.	3. Recipient's Catalog No.
79537		

4. Title and Subtitle	5. Report Date
A Beaming Model of the Io-Independent Jovian Decameter Radiation Based on Multipole Models of the Jovian Magnetic Field	April 1978
	6. Performing Organization Code
7. Author(s)	8. Performing Organization Report No.
Melvyn L. Goldstein, Aharon Eviatar, and James R. Thieman	
9. Performing Organization Name and Address	10. Work Unit No.
Laboratory for Extraterrestrial Physics NASA/Goddard Space Flight Center Greenbelt, Maryland 20771	11. Contract or Grant No.
	13. Type of Report and Period Covered
12. Sponsoring Agency Name and Address	Technical Memorandum
	14. Sponsoring Agency Code

15. Supplementary Notes

16. Abstract

A geometrical model is presented in which the apparent source locations of the Io-Independent decameter radiation are computed. The calculations assume that the radiation is produced by stably trapped electrons radiating near the local electron gyrofrequency and that the emission is then beamed onto a conical surface. The maximum occurrence probability of noise storms is associated with regions in the Jovian magnetosphere where the axis of the emission cone is most inclined toward the Jovian equatorial plane. The calculations utilize and compare two of the octupole spherical harmonic expansions of the Jovian magnetic field constructed from data accumulated by the fluxgate and vector helium magnetometers on board Pioneer 11.

17. Key Words (Selected by Author(s))	18. Distribution Statement
Jupiter, Decameter Radiation, Loss-Cone Instability	Unlimited

19. Security Classif. (of this report)	20. Security Classif. (of this page)	21. No. of Pages	22. Price*
Unclassified	Unclassified	39	

*For sale by the National Technical Information Service, Springfield, Virginia 22151.